Materials Advances

ROYAL SOCIETY OF CHEMISTRY

PAPER

View Article Online
View Journal | View Issue

Check for updates

Cite this: *Mater. Adv.*, 2020, 1, 3406

Silsesquioxane-based and triptycene-linked nanoporous polymers (STNPs) with a high surface area for CO_2 uptake and efficient dye removal applications†

Akhtar Alam, Atikur Hassan, Ranajit Bera and Neeladri Das *

Received 3rd September 2020,
Accepted 28th October 2020

DOI: 10.1039/d0ma00672f

rsc.li/materials-advances

A unique set of polymers were conveniently obtained by marriage of 'cubic' octavinylsilsesquioxane (OVS) and 'paddle wheel' shaped triptycene using the simple and economical Friedel–Crafts reaction. The resulting 'hybrid inorganic–organic polymers' (STNPs) are nanoporous with higher surface areas than several previously reported porous polymeric networks containing either one of the two structural motifs (OVS or triptycene). In addition, the STNP with the highest surface area (**STNP3**) also has better gas storage and dye capture abilities than several organic adsorbents derived from silsesquioxanes. The performance of **STNP3** as a dye adsorbent suggests that it can be further explored for environmental remediation.

Introduction

The design and synthesis of porous materials having a high surface area has excited researchers globally due to their versatile applications which include (but are not limited to) the selective uptake of small gas molecules (CO_2, CH_4, and H_2),[1–3] heterogeneous catalysis[4] and efficient sorbents for toxic pollutants.[5] Among porous materials, the ones derived from organic monomers are especially attractive because of their convenient synthesis, easy functionalization, facile tuning of porous properties (surface area, pore size, total pore volume, *etc.*) and excellent stability. These are popularly referred in contemporary literature as Covalent Organic Frameworks (COFs)[6–9] and Porous Organic Polymers (POPs).[10–13]

Silsesquioxanes are three dimensional oligomers and are generally represented as $(RSiO_{1.5})_{2n}$. Depending on the R group (such as phenyl, vinyl, propyl – to name a few) these exhibit unique and interesting properties.[14] Polyhedral oligomeric silsesquioxanes (POSSs) having the general formula $(RSiO_{1.5})_8$ are a subclass of silsesquioxanes.[15] In contemporary research, POSS moieties have received substantial research attention. These have been incorporated in various polymeric networks to yield hybrid inorganic–organic materials that are thermally stable, resistant to chemicals, non-toxic and biocompatible in nature.[16–18] If the R group is vinyl, the resulting POSS is termed as octavinylsilsesquioxane (OVS) and is represented by the formula $(C_2H_3)_8Si_8O_{12}$. OVS is commercially available and has been reported as one monomer/cross-linking agent in the design of several new hybrid (inorganic/organic) materials for versatile applications. Polymeric networks derived from OVS monomers are porous materials that have potential application in selective capture and storage of CO_2 as well as adsorbents for toxic dyes present in industrial effluents.[19–22] OVS derived porous materials may also be promising materials for light-harvesting applications,[23] catalysis, photo-voltaic or electronic devices,[24,25] and sensors for explosive detection.[26–28] Such silsesquioxane based hybrid porous materials can be conveniently synthesized using various synthetic strategies that include (but are not limited to) the Friedel–Crafts reaction,[26,29] hydrosilylation,[30] and coupling reactions such as the Heck reaction,[17,31] Sonogashira[32] and Yamamoto.[33] While most coupling reactions employ expensive transition metal catalysts and rigorous reaction conditions, the use of Friedel–Crafts reaction conditions makes the polymerization facile, economical as well as versatile. Friedel–Crafts reaction conditions were also applied for the facile and 'large-scale' production of porous materials.[34]

Triptycene is an organic molecule with a bicyclic ring in its core. It has three peripheral phenyl rings that are suitably oriented to provide multiple crosslinking sites when used as one of the monomers in the Friedel–Crafts reaction.[35–37] Network polymers derived from triptycene are porous materials.[38] The presence of micropores and the associated high surface areas are attributed to the three-dimensional and contorted structure of triptycene motifs present in the polymeric backbone.[38–40]

Department of Chemistry, Indian Institute of Technology Patna, Patna 801106, Bihar, India. E-mail: neeladri@iitp.ac.in, neeladri2002@yahoo.co.in; Tel: +91 9631624708

† Electronic supplementary information (ESI) available. See DOI: 10.1039/d0ma00672f

Triptycene-based microporous organic polymers are also reported to demonstrate interesting applications in materials chemistry, such as small gas molecules (CO_2, H_2, CH_4 and N_2) capture and separation (CO_2/CH_4, CO_2/N_2 and CH_4/N_2),[41–45] toxic dye removal and iodine adsorption for environmental remediation.[46–51]

Thus it is expected that the material incorporating triptycene and octa-functional OVS would yield a highly porous network. It is desirable that such materials should also have the potential to selectively capture carbon dioxide and toxic organic dyes for environmental remediation. These are in line with the objective to develop/obtain novel hyper-crosslinked polymers (with improved properties) synthesized from inexpensive monomers. It is also expected that such polymers have desirable properties such as high porosity and surface area, and high stability. Furthermore, it was anticipated that the ratio of the two monomers (*i.e.*, triptycene and OVS) would be crucial in the fine tuning of the porosity of the resultant silsesquioxane based hybrid porous materials. With these premises in mind, the objective was to obtain a set of unique triptycene based porous polymers bearing OVS moieties using the Friedel–Crafts reaction.

For the first time, herein we report the marriage of triptycene and polyhedral silsesquioxanes (in the form of OVS) to yield a set of four unique silsesquioxane-based and triptycene-linked hybrid nanoporous polymers (STNPs). By varying the molar ratio of triptycene and OVS, **STNP1**, **STNP2**, **STNP3**, and **STNP4** were obtained with multimodal porosity. Thus using this strategy, it was easily possible to tune the porous properties and surface area of the resulting polymeric network. Subsequently, the STNPs' ability to capture small gases was studied. Finally, the STNPs were tested as adsorbents for common organic dyes that are often used in the textile industry and are present in industrial effluents as toxic pollutants above restricted levels.

Results and discussion

Using various molar ratios of triptycene and OVS dissolved in 1,2-dichloroethane and in the presence of anhydrous aluminium chloride, a set of four STNPs were conveniently prepared (Scheme 1) in high yields (85–92%). STNPs were obtained as yellow powder and these are insoluble in common organic solvents. It is also reported by others that such hybrid porous polymeric networks are insoluble in common organic solvents.[20,29]

STNPs (**1–4**) thus obtained were structurally characterized using FTIR and ^{13}C CP-MAS NMR spectroscopies. In the respective FTIR spectrum, the incorporation of OVS units in STNPs was evident from the presence of a strong peak at 1103 cm^{-1} which is observed due to Si–O–Si stretching vibrations (Fig. 1). Additionally, the signal at 780 cm^{-1} is due to Si–C bond vibration.[52] These signals are signature peaks observed in the FTIR spectrum of materials having silsesquioxane units.[53,54] A comparison of FTIR spectra of triptycene and OVS with those of STNPs shows that the intensities of peaks between 1292 cm^{-1} and 1608 cm^{-1} (prominently seen in monomers) had decreased considerably in the STNPs. This suggested the successful Friedel–Crafts alkylation reaction between vinyl groups (in OVS) and phenyl rings (in triptycene motifs). Consequently, a decrease in intensity and sharpness of C–H stretching (in triptycene) at around 3000 cm^{-1} was also observed in the resulting STNPs with the simultaneous increase in methylene signal at around 2923 cm^{-1}. Thus FTIR spectral analysis suggested the successful cross-linking reaction between triptycene and OVS as depicted in Scheme 1.

The formation of the desired STNPs was also confirmed from the analysis of their corresponding ^{13}C CP-MAS NMR spectrum. The ^{13}C solid-state CP-MAS spectrum of **STNP3** is shown in Fig. 2 as a representative example. The signal appearing at around 52 ppm was due to the bridgehead carbons present in the triptycene unit and this has been observed in NMR spectra of polymers having triptycene motifs.[55–57] In addition, signals due to the carbons present in the arene rings were observed in between 127 and 147 ppm. The resonance peaks around 27 and 17 ppm are assigned to the ethylene carbons connecting the Si atom on one side and a triptycene-based arene ring on the other side. Thus, solid ^{13}C CP-MAS NMR (Fig. 2) data also confirmed the successful crosslinking between triptycene and OVS (Scheme 1).

The morphologies of STNPs were characterized by field emission scanning electron microscopy (FESEM). Fig. 3 shows

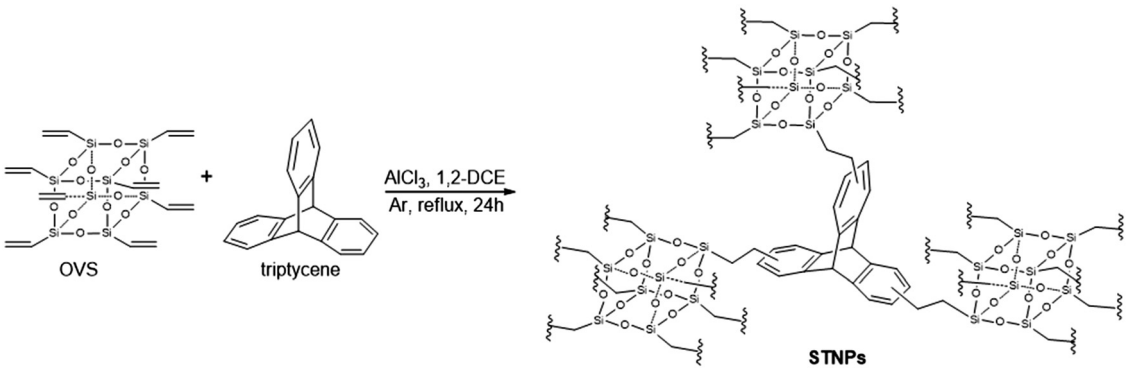

Scheme 1 Synthesis of STNPs.

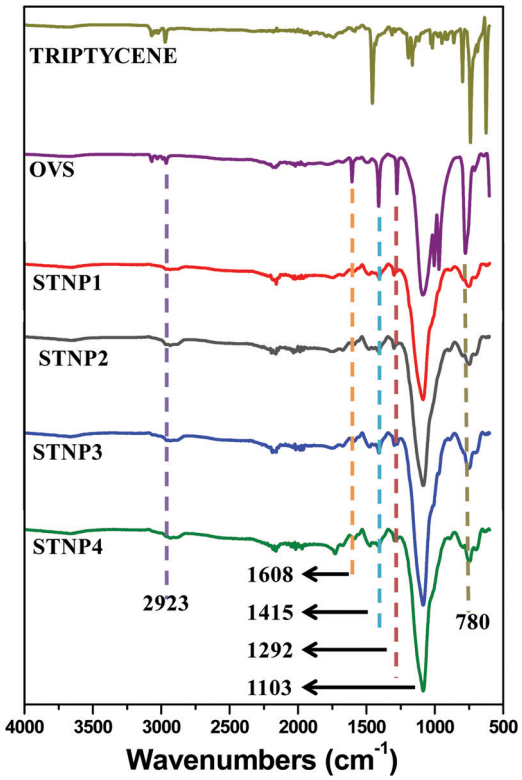

Fig. 1 FTIR spectra of triptycene, OVS and **STNP 1–4**.

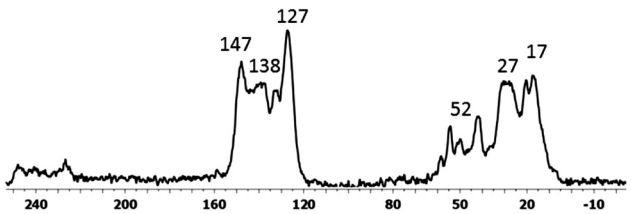

Fig. 2 Solid-State ^{13}C CP-MAS NMR spectra of **STNP3**.

the FESEM image of **STNP3** as a representative example and images of the other three STNPs are included in the ESI† (Fig. S1). The morphologies observed for all STNPs have similar characteristics such as non-uniform aggregates of various sizes. Such a wide distribution in size was also observed in the previously reported hybrid polymers incorporating OVS units. The presence of the Si element due to the inclusion of OVS units in **STNP3** was further confirmed from the EDX (Energy Dispersive X-ray) data (Fig. 3).

The PXRD data of the STNPs were also recorded and are shown in Fig. 4. While it is well known that OVS is crystalline, the polymers (STNPs) resulting due to crosslinking of triptycene and OVS are amorphous in nature. This shows that polymerization results from the loss of the crystalline nature of POSS. The observed amorphous nature of STNPs is due to the randomness in the distribution of OVS units and the presence of triptycene units in the matrix of STNPs. The presence of Si–O–Si linkages due to the presence of OVS motifs in STNPs was clearly indicated from the presence of the broad peak centered at 2θ equal to 22°.[58,59]

Porosity measurements

The N_2 adsorption–desorption isotherms were recorded at 77 K for each STNP in order to obtain useful information regarding their porous properties such as surface area, pore size distribution and total pore volume. The sorption isotherms (Fig. 5) indicate that while the uptake of nitrogen by each STNP is reasonably high at low relative pressures (P/P_0 = 0 to 0.02), it is rather low in the mid and relatively higher pressure ranges up to P/P_0 = 1. In each case, the reversible isotherms feature a hysteresis loop which is considered as a sign of the existence of the nanoporous structure, *i.e.*, the simultaneous presence of micropores and mesopores defining the porous structure.[60] The presence of a distinct hysteresis loop also suggests that these are type IV reversible isotherms. From these features of the isotherms, it may be stated that in the case of STNPs, capillary condensation takes place in their mesopores leading to restriction in the extent of gas capture in the relatively higher P/P_0 range. The shape of the hysteresis loop closely resembles that of type H4, since the adsorption and desorption branches are nearly horizontal over a wide range of relative pressure (P/P_0). According to IUPAC, porous materials (like STNPs) that exhibit 'type H4' loop have considerable narrow pores that are 'slit-shaped'.[61]

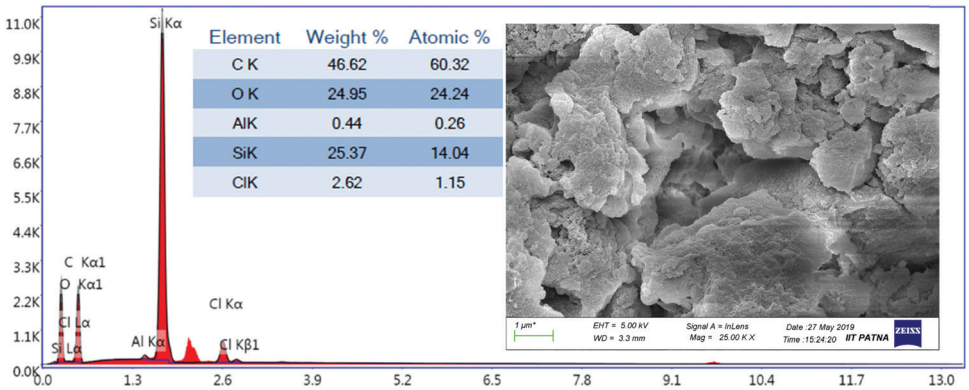

Fig. 3 FESEM image with EDX of **STNP3**.

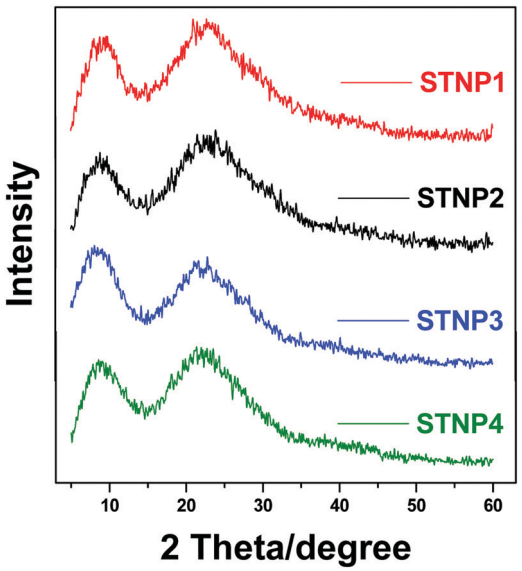

Fig. 4 PXRD pattern for OVS incorporated STNPs.

The Brunauer–Emmett–Teller (BET) model is most appropriate to estimate the surface area of a porous material if it shows a type IV isotherm. Thus the BET model was applied to estimate the surface areas (SA_{BET}) associated with STNPs and these were found to be 1256 $m^2\ g^{-1}$ (**STNP1**), 1421 $m^2\ g^{-1}$ (**STNP2**), 1462 $m^2\ g^{-1}$ (**STNP3**) and 1271 $m^2\ g^{-1}$ (**STNP4**). The corresponding Langmuir surface areas for **STNP1**, **STNP2**, **STNP3** and **STNP4** are 1956 $m^2\ g^{-1}$, 2266 $m^2\ g^{-1}$, 2300 $m^2\ g^{-1}$ and 1941 $m^2\ g^{-1}$, respectively (Table 1 and Fig. S2, S3, ESI†). Among the four polymeric networks reported herein, **STNP3** shows the highest surface area. The magnitude of surface area is better than that reported for most of the other silsesquioxane-based porous hybrid materials reported to date, such as the silsesquioxane-based thiophene-bridged network (915 $m^2\ g^{-1}$ for THPP),[17] the ferrocene-functionalized silsesquioxane-based polymer (1015 $m^2\ g^{-1}$ for Fc-HPP),[62] luminescent porous organosilicon polymers (1003 $m^2\ g^{-1}$ for LPOP-2),[26] hybrid polymers constructed from octavinylsilsesquioxane and benzene (904 $m^2\ g^{-1}$ for HPP-3),[29]

Table 1 Porous properties of STNPs

Polymers	Molar ratio OVS : Trip	SA_{BET} ($m^2\ g^{-1}$)	SA_{Lang}[a] ($m^2\ g^{-1}$)	V_{total}[b] [$cm^3\ g^{-1}$]
STNP1	1.0 : 0.53	1256	1956	1.377
STNP2	1.0 : 0.86	1421	2266	1.167
STNP3	1.0 : 1.0	1462	2300	1.096
STNP4	1.0 : 1.5	1271	1941	0.855

Surface area of STNPs calculated based on the BET model and the Langmuir model[a] from the N_2 adsorption isotherms (P/P_0 = 0.05–0.35). The total pore volume[b] of STNPs calculated at P/P_0 = 0.99.

octavinylsilsesquioxane-based luminescent hybrid polymers (685 $m^2\ g^{-1}$ for PS-3)[23] and polyhedral oligomeric silsesquioxane-based polymers (778 $m^2\ g^{-1}$ for HPP-2).[63] However, the SA_{BET} of **STNP3** is lower than silsesquioxane-based tetraphenylethene-linked polymers (1910 $m^2\ g^{-1}$) which to our knowledge is the highest value observed for a silsesquioxane-based POP.[20] The surface area of **STNP3** is also better than various triptycene based hyper-cross-linked polymers reported in the literature such as nanoporous organic polymers (1246 $m^2\ g^{-1}$ for NOP-47),[64] porous organic copolymers with triptycene and crown ether (848 $m^2\ g^{-1}$ for POP-TCE-15),[48] triptycene based hyper-cross-linked polymer sponge (1426 $m^2\ g^{-1}$ for THPS),[35] and triptycene based microporous polymers (1372 $m^2\ g^{-1}$ for TMP3).[36]

Next, the pore size distribution (PSD) plots for STNPs were obtained from the N_2 sorption isotherms by using the density functional theory (DFT) method. These curves (Fig. 5) indicated multimodal distribution with peaks centered in both microporous (around 1.5 nm) and mesoporous regions (between 2.5–6 nm). The pore-size distribution is relatively thinner in the microporous region (below 2 nm) than that in the mesoporous region. The difference in the shape of the PSD plots for STNPs implies that the molar ratio of triptycene and OVS is an important parameter that governs the pore structure of the resultant silsesquioxane-based and triptycene-linked hybrid polymers. Considering the presence of both micropores and mesopores, STNPs can be classified as nanoporous materials. The porosity data of STNPs are compiled in Table 1 for comparison. The total pore volume of each STNP was calculated

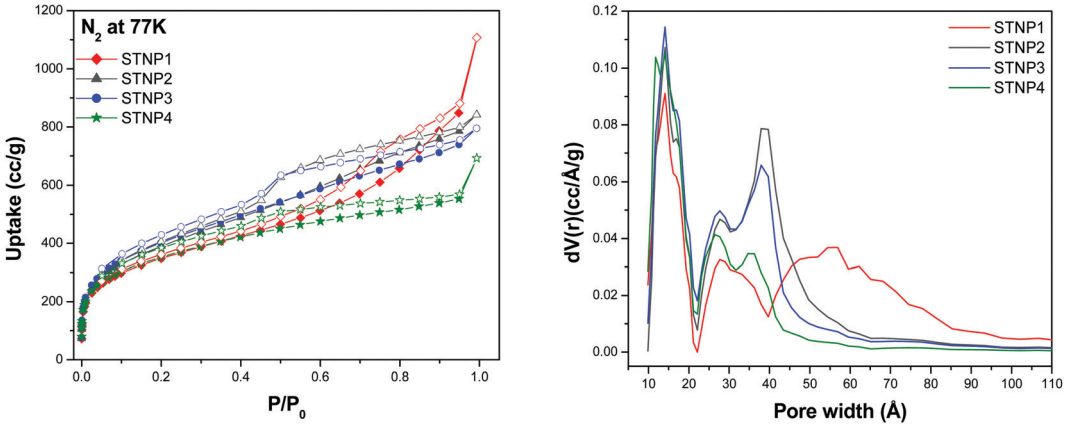

Fig. 5 N_2 adsorption–desorption isotherms at 77 K (left) and pore size distribution (right) of STNPs.

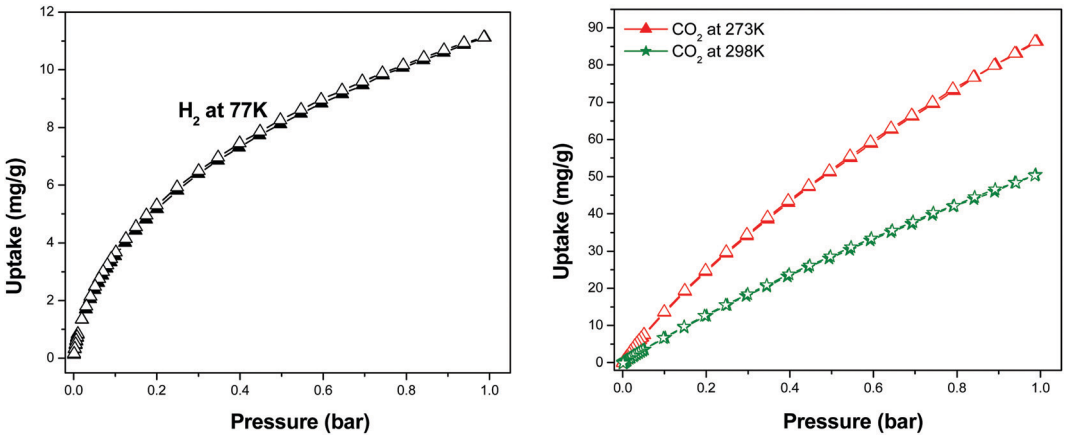

Fig. 6 H_2 and (left) and CO_2 (right) sorption isotherms of **STNP3** (filled triangle/star = adsorption and empty triangle/star = desorption)

from the volume of N_2 adsorbed at $P/P_0 = 0.99$ and this parameter was measured to be 1.377 cc g^{-1} for **STNP1**, 1.167 cc g^{-1} for **STNP2**, 1.096 cc g^{-1} for **STNP3** and 0.855 cc g^{-1} for **STNP4**.

The data presented in Table 1 indicate that the magnitude of various porosity parameters of STNPs can be easily altered by changing the molar ratio of OVS and triptycene. Interestingly, the highest surface area (SA_{BET} = 1462 m^2 g^{-1}) was observed in the product (**STNP3**) that utilized equimolar quantities of OVS and triptycene in the polymerization reaction. A lower surface area was recorded when the OVS : triptycene molar ratio was either less or more than unity. These observations may be justified by considering that each triptycene molecule has three phenyl rings that connect multiple OVS to form STNPs. At a lower concentration of triptycene, it might be possible that all the vinyl groups present in OVS units are not linked to the phenyl rings of triptycene leading to a relatively lower BET surface area. As the concentration of triptycene units increases (**STNP1** < **STNP2** < **STNP3** < **STNP4**), the vinyl rings (of OVS) covalently crosslink with the phenyl rings of triptycene to a greater extent. This results in higher surface area of the resulting polymeric network due to greater crosslinking. Thus the surface area increases as the OVS : triptycene ratio decreases from 1.89 (**STNP1**) to 1.0 (**STNP3**). Further decrease in the OVS : triptycene ratio to 0.67 (**STNP4**) results in a decrease in SA_{BET}. This implies that at such higher concentrations of triptycene, all phenyl rings of triptycene might not act as connecting sites and hence local crosslinking densities will not keep increasing. This effect may be also related to steric hindrance preventing further increase in SA_{BET} in the case of excess triptycene units used in **STNP4**. Hence, relative to **STNP3**, a further increment in the surface area is not observed in **STNP4**. The overall decrease in the total pore volume with a decrease in the OVS : triptycene ratio might be due to more interpenetration of the framework since all triptycene phenyl rings might not participate in crosslinking leading to the pore-filling of the network to some extent. To sum up, the flexible nature of Si–CH_2–CH_2–Ar and the rigid bulky structure of triptycene contribute to the observed trend in the porous properties of STNPs (Table 1).

Gas storage

STNPs reported herein have rich porous properties. Hence it was our research interest to evaluate their performance as an adsorbent for small gaseous molecules (H_2, N_2 and CO_2) and compare the results with the previously reported hybrid materials derived from OVS and triptycene derivatives. Among the four polymeric networks (**STNP 1–4**) that possessed similar chemical linkages, **STNP3** was selected to explore its gas storage capacity since it had exhibited the highest surface area (SA_{BET} = 1462 m^2 g^{-1}). Gas sorption experiments using H_2 (at 77 K) and CO_2 (at 273, 298 K) were performed at the pressures up to 1 bar. The H_2 uptake for **STNP3** was 11.1 mg g^{-1} (1.11 wt%) at 1 bar (Fig. 6). The H_2 adsorption capacity was comparable and better than that reported for other silsesquioxane-based porous hybrid materials in general and OVS in particular. Representative examples include (but are not limited to) hybrid polymers constructed from octavinylsilsesquioxane and benzene (HPP-3, 0.70 wt%),[29] hybrid porous polymers (HPPs), derived from octavinylsilsesquioxane and tetraphenylsilane (HPP-5, 0.80 wt%),[65] hybrid nanoporous polystyrene derived from octavinylsilsesquioxane and polystyrene (HCP-3, 0.60 wt%).[66] From the above literature comparisons, it is clear that **STNP3** reported herein has improved H_2 uptake capabilities than those of several silsesquioxane-based porous hybrid materials. We attribute this to the simultaneous incorporation of triptycene motifs that are associated with internal free volume (IFV).[67]

Next, the ability of the triptycene-linked hybrid and porous **STNP3** to selectively capture CO_2 was tested. Considering the harmful effects of global warming due to CO_2 gas emitted from anthropogenic sources such as thermal power plants, assessing CO_2 storage properties of porous materials has assumed industrial importance. A major technological challenge is to develop efficient thermally stable adsorbents to reduce atmospheric CO_2 emissions from coal powered plants. Several recently published articles have highlighted the importance of hybrid porous materials as an adsorbent for CO_2.[20] With this background, it was our interest to evaluate STNPs as materials for CO_2 uptake and compare their performance with other OVS derived polymeric networks. Thus, CO_2 sorption isotherms

were recorded at two temperatures (273 K and 298 K) and at pressures up to 1 bar (Fig. 6) for **STNP3**. The gravimetric uptake of CO_2 for **STNP3** was 86 mg g^{-1} (8.60 wt%) at 273 K and 50 mg g^{-1} (5.0 wt%) at 298 K. Compared to some previously reported silsesquioxane based hybrid porous materials, the performance of **STNP3** for CO_2 uptake had improved. Representative examples of polymers with a lower CO_2 uptake include (but are not limited to) silsesquioxane-based tetraphenylethene-linked polymers (HPP-3, 6.25 wt% at 273 K),[20] silsesquioxane-based triphenylamine functionalized polymer, (HLPP-OTS, 8.04 wt% at 273 K),[19] ferrocene-functionalized silsesquioxane-based polymer (Fc-HPP, 4.87 wt% at 273 K),[62] hybrid polymers derived from octavinylsilsesquioxane and polystyrene (HCP-3, 4.93 wt% at 298 K),[66] hybrid polymers constructed from octavinylsilsesquioxane and benzene (HPP-3, 2.73 wt% at 298 K),[29] hybrid porous polymers derived from octavinylsilsesquioxane and tetraphenylsilane (HPP-5, 3.31 wt% at 298 K).[65] We attribute such marked improvement in our OVS based hybrid porous polymer (**STNP3**) to the concurrent incorporation of rigid and three-dimensional contorted triptycene units having internal free volume along with OVS.

The Q_{st} (isosteric heats of adsorption) value of **STNP3** for CO_2 uptake was directly calculated from the experimental adsorption isotherms collected at 273 and 298 K using the Clausius–Clapeyron relation. The Q_{st} values for CO_2 were observed in the range 22.0 kJ mol^{-1} at zero coverage (Fig. S4, ESI†). Magnitude of Q_{st} provides valuable insight regarding the nature and extent of interaction (strength) between the adsorbent and the adsorbate. The Q_{st} value recorded for CO_2 capture by **STNP3** suggests uptake *via* a physisorption process because the magnitude (of Q_{st}) is less than 40 kJ mol^{-1}.[68] This Q_{st} value of CO_2 capture by **STNP3** is less than that for a previously reported porous polymer (HPP-1c) obtained using OVS and 2,2′,7,7′-tetrabromo-9,9′-spirobifluorene.[25] This suggests that **STNP3** has better potential for use as a porous adsorbent with 'reversible' CO_2 uptake. The ability of **STNP3** to selectively capture CO_2 over N_2 was also examined. The CO_2/N_2 selectivity was calculated in the pressure range of 0–0.1 bar, using the Henry law and on the basis of initial slope calculations (Fig. S5, ESI†). **STNP3** showed CO_2/N_2 selectivity of 20 at 273 K and 11 at 298 K.

Dye adsorption

The contamination of water with various pollutants is a serious environmental issue.[69–71] Organic dyes are a class of toxic water soluble pollutants that need to be eliminated from industrial effluents prior to discharge into water bodies. Among the various strategies known, the technique of adsorbing the dye molecules using a suitable adsorbent is the most popular because it is a simple and economical technique.[72–74] Considering the highest surface area of **STNP3**, it was selected for estimating its potential as an adsorbent for certain common dyes that are also considered as water pollutants. The dyes selected in this study included cationic [methylene blue (MB), rhodamine B (RB) and crystal violet (CV)] as well as anionic dyes [congo red (CR) and methyl orange (MO)]. The physical and chemical properties of the dyes are summarized in Table S1 (ESI†).[35,75,76] The adsorption capacities of **STNP3** for various dyes were measured by recording respective adsorption isotherms. Aqueous solutions of the dye were prepared in various concentrations (100–1600 ppm) using deionized water. To a 4 mL solution of a dye of certain concentration, 4.0 mg of **STNP3** was dispersed by continuous stirring at 600 rpm for 24 hours at room temperature. The equilibrium adsorption capacity (Q_e) and the removal efficiency were calculated using the following eqn (1) and (2) for various concentrations (C_e) of each dye solution.

$$Q_e = \frac{(C_0 - C_e) \times V}{M} \quad (1)$$

$$\text{Removal efficiency } (\%) = \frac{C_0 - C_e}{C_e} \times 100\% \quad (2)$$

Herein, C_0 represents the initial concentration of the dye, C_e is the equilibrium concentration of the dye, V denotes volume of the dye solution and M is the weight of the adsorbent.

The dye adsorption data (Fig. 7) show that Q_e for **STNP3** increases significantly as the initial dye concentration is increased.

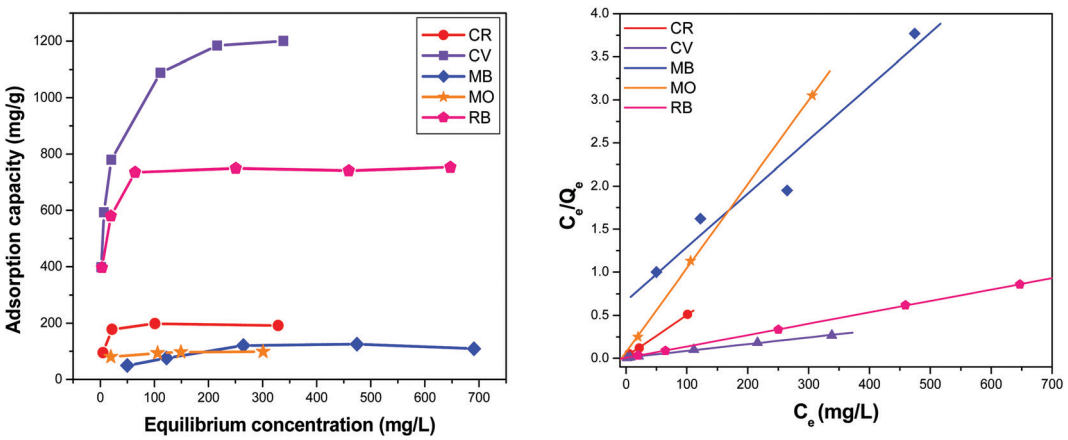

Fig. 7 Equilibrium adsorption isotherms (left) and linear fitting of the equilibrium data by using the Langmuir Equation (right) of dyes on **STNP3**.

However, with further increase in dye concentrations, adsorption saturation is reached for **STNP3**. The maximum value of Q_e obtained was 198 mg g^{-1} for CR, 1261 mg g^{-1} for CV, 135 mg g^{-1} for MB, 106 mg g^{-1} for MO and 752 mg g^{-1} for RB. In order to describe the mechanism of dye adsorption by **STNP3**, the Langmuir and Freundlich adsorption models were applied. The Langmuir isotherm model is described by eqn (3) and assumes energetically identical and non-interacting adsorption sites as well as monolayer adsorbate coverage on the surface. The Freundlich isotherm model is defined by eqn (4), in which case, the adsorption is non-ideal since adsorption sites are non-identical with varied affinities for adsorbate species. Unlike the Langmuir model, the Freundlich model assumes non-homogenized and multilayer adsorption.[77,78]

The equations corresponding to these two classical adsorption models were employed to fit the equilibrium data of dye adsorption by **STNP3** (Fig. 7 and Fig. S6, ESI†). The respective magnitudes of adsorption constants and the correlation coefficients (R^2), calculated for both isotherm models are presented in Table 2. The correlation coefficients of the Langmuir isotherm model ($R_L{}^2$, 0.999 for CR, 0.997 for CV, 0.994 for MB, 0.999 for MO and 0.999 for RB) are higher than those calculated for the Freundlich isotherm model ($R_F{}^2$, 0.918 for CR, 0.981 for CV, 0.957 for MB, 0.975 for MO and 0.938 for RB). This implies that the Langmuir isotherm model has a better fit with the experimental data and adsorption of dyes on the surface of **STNP3** is monolayer adsorption. It also suggests that the dye adsorption sites in **STNP3** are more or less uniform and identical.

$$\frac{C_e}{Q_e} = \frac{C_e}{Q_m} + \frac{1}{Q_m K_L} \quad (3)$$

$$\ln Q_e = \ln K_F + \frac{1}{n} \ln C_e \quad (4)$$

where C_e (mg L^{-1}) is the equilibrium concentration, Q_e (mg g^{-1}) is the equilibrium adsorption capacity, Q_m (mg g^{-1}) is the maximum adsorption capacity of the Langmuir isotherm model, K_L (L mg^{-1}) is a Langmuir adsorption coefficient, K_F (L mg^{-1}) is the Freundlich constant, and $1/n$ is an indicator that reflects the nonlinear degree of adsorption.

From the Langmuir plot, the maximum adsorption capacity (Q_m) can be computed and was found to be 1428 mg g^{-1} for CV, 1000 mg g^{-1} for RB, 250 mg g^{-1} for CR, 166 mg g^{-1} for MB and 111 mg g^{-1} for MO. These calculated values of Q_m are slightly higher than the corresponding experimental Q_e values. The values of Q_m obtained for CV and RB are significantly higher than those for the other dyes used in this study. Furthermore, from these Q_m data, **STNP3** is a better adsorbent for CV and RB than several other porous polymeric networks reported previously. The comparison of dye adsorption data of **STNP3** with those of other materials is provided in Table S2 (ESI†).

Table 2 Summary of the Langmuir and Freundlich isotherm model parameters for the adsorption of dyes using **STNP3** as an adsorbent

		Langmuir constants			Freundlich constants		
Dyes	Nature	Q_m (mg g^{-1})	K_L (L mg^{-1})	$R_L{}^2$	K_F (L mg^{-1})	n	$R_F{}^2$
CR	Anionic	250	0.182	0.999	69.40	4.06	0.918
CV	Cationic	1428	0.087	0.997	368.70	4.54	0.981
MB	Cationic	166	0.009	0.994	17.28	3.51	0.957
MO	Anionic	111	0.125	0.999	63.43	12.82	0.975
RB	Cationic	1000	0.20	0.999	372.41	8.77	0.938

From the results of these experiments, it follows that the adsorption capacity of **STNP3** for various dyes decreases in the order CV > RB > CR > MB > MO. These dye molecules have different molecular sizes.[35,75,76] Thus, it can be concluded that **STNP3** shows size-selective dye adsorption. The PSD profile of **STNP3** shows that this polymer has micropores as well as mesopores. As far as the charge associated with these dyes is concerned, CV, RB and MB are cationic, while CR and MO are anionic. Among the five dyes used in this study, CR has the largest molecular size while MO has the smallest. RB and CV have similar size and have a diameter greater than 1.5 nm.[62] On the other hand, MB and MO are relatively smaller in size and their diameters are less than 1.5 nm.

In the present study, **STNP3** has much higher affinities for the two larger sized cationic dyes (CV and RB) relative to the smaller cationic dye (MB). As far as the anionic dyes (CR and MO) are concerned, **STNP3** has a rather poor affinity for the anionic CR molecules even though CR has the biggest molecular size. From their structural composition, POSS cores are rich in electronegative oxygen atoms and thus they have a natural tendency to capture cationic dyes such as CV and RB *via* favorable electrostatic attractive interactions. The observed lower adsorption capacity in the case of anionic dyes is due to repulsive ion–dipole interaction between these dyes (CR and MO) and the electronegative inorganic silsesquioxane cores present in **STNP3**. Additionally, the correlation between the pore structure of **STNP3** and the size of the dyes also supports the observed absorption capacity (CV > RB > CR > MB > MO). The larger dye molecules (CR, RB and CV) either clog the small micropores upon binding or interact well with the mesopores. The relatively smaller dyes (MB and MO) enter and exit the larger sized micro- and mesopores easily due to their smaller size (diameter < 1.5 nm) and hence these are adsorbed to a much smaller extent even though MB is cationic. Overall, the trend in absorption capacity of various dyes depends on the simultaneous interplay of several factors such as the porous structure and surface area of the adsorbent, the ionic nature of the dye (adsorbate) and groups present in the polymeric framework of the adsorbent.

Considering the high Q_m value of RB and CV, it was assumed that **STNP3** may be a potential adsorbent for these two dyes for practical applications. Therefore, it was our interest to further explore their adsorption kinetics using **STNP3** as an adsorbent. While using RB as an adsorbate, the experiment was done by adding 10 mg **STNP3** into 10 mL aqueous RB solution with an initial concentration of 40 ppm. The CV adsorption kinetics was checked by adding 10 mg **STNP3** into 10 mL aqueous CV solution with an initial concentration of 100 ppm. Dye absorption kinetics was monitored by recording the visible

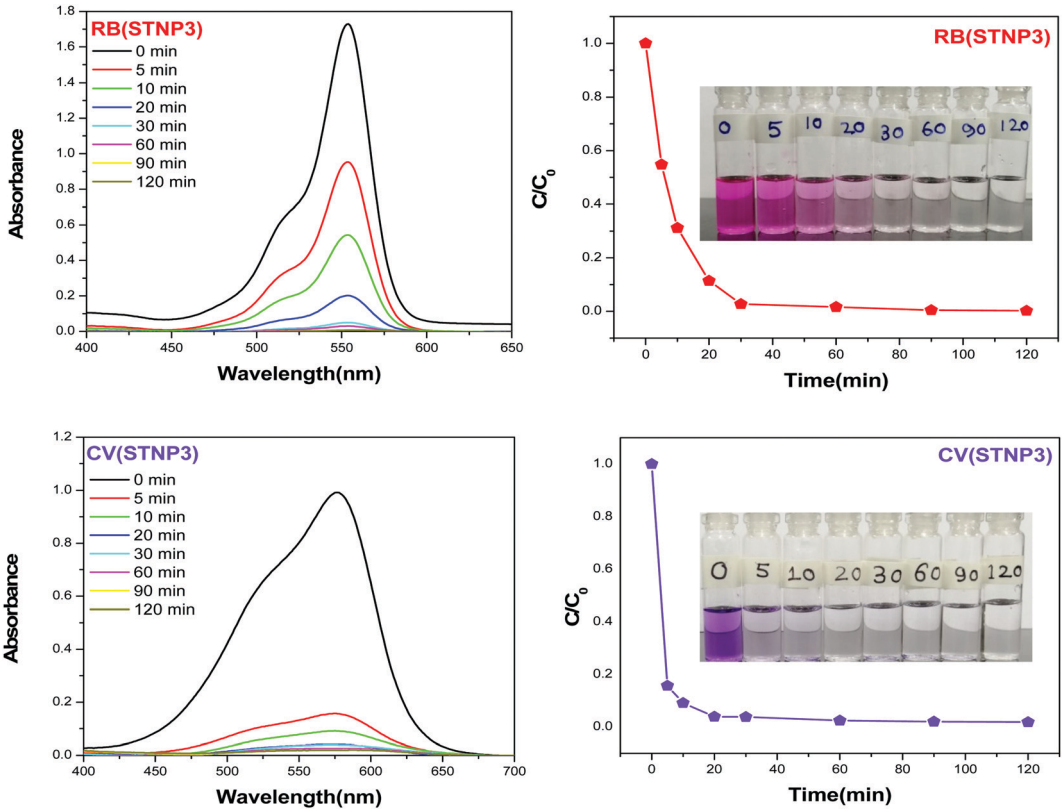

Fig. 8 UV-Vis absorption spectra of the RB and CV solutions after being treated with **STNP3** at different time intervals; the initial concentration of the RB and CV solutions being 40 ppm and 100 ppm, respectively (left); adsorption rates of RB and CV using **STNP3**, the insets show the corresponding digital camera images (right).

spectrum at different time intervals. The adsorption spectra were recorded at different time intervals and are shown in Fig. 8. The gradual adsorption of dyes with time could be also visualized by the naked eyes (inset of Fig. 8). It was observed that with the onset of the experiment, the adsorption rate is fast and the uptake rate slows down with the progress of time. For **STNP3**, within 10 min, the removal efficiency reached 70% for RB and 90% for CV. The time taken for nearly complete removal of RB is around 30 min and that for CV is even less, at around 20 min.

Recyclability of STNPs

Recyclability is a desirable trait in the case of porous materials as efficient adsorbents from an economical perspective. The recyclable nature of **STNP3** as an adsorbent was evaluated through repeated adsorption–desorption experiments and the performance is shown in Fig. 9. In each cycle, the **STNP3** sample (loaded with either CV or RB) was regenerated by repeated extraction of the adsorbed dye using hot methanol and 2 M hydrochloric acid for approximately 12 hours.[22] The sample of **STNP3** thus obtained was next dried under vacuum at 120 °C for several hours. The regenerated mass of **STNP3** was weighed precisely and reused for another cycle of dye adsorption. A decrease in dye removal efficiency (contact time: 10 min) was observed at the end of the fifth cycle to the extent of 71% (from 90%) for CV and 58% (from 70%) for RB. The small loss

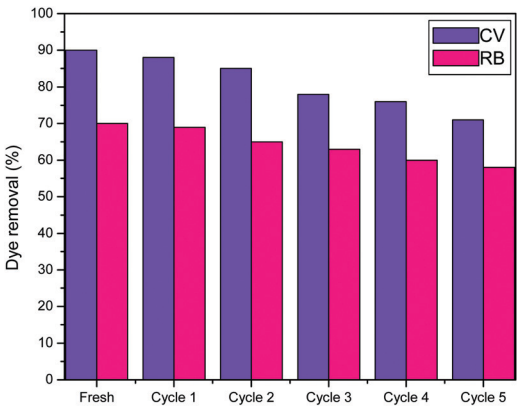

Fig. 9 Reusability of **STNP3** for removing CV and RB (contact time = 10 min).

in the dye adsorption ability of **STNP3** is probably due to the strong interaction between the dye molecules and **STNP3.** Some of these large sized dye molecules (CV or RB) may get trapped in the small micropores so that their complete removal during extraction is not possible. Consequently, there is a small decrease in the adsorption ability of **STNP3** after each regeneration cycle. Nevertheless, these experiments suggest that **STNP3** may be used as an efficient dye adsorbent for several cycles.

Conclusions

In summary, the synthesis of a unique set of OVS based and triptycene motif incorporated 'hybrid inorganic–organic' polymeric materials has been described. These silsesquioxane-based and triptycene-linked nanoporous polymers (STNPs) were obtained in high yields *via* the well-known Friedel–Crafts reaction that used a cost-effective catalyst. The simultaneous incorporation of these two structural motifs, *i.e.*, cubic OVS and propeller shaped triptycene, resulted in the formation of porous materials with reasonably superior surface areas when compared with a majority of the previously reported silsesquioxane based polymers. The polymer with the highest surface area (**STNP3**) has superior gas storage and dye capture abilities when compared with several other organic adsorbents derived from silsesquioxanes. More importantly, the dye adsorption efficiency of **STNP3** is dependent not only on the size of the dye but also on the charge associated with it. The results indicate that the maximum adsorption capacity (Q_m) of **STNP3** is remarkably higher for bulkier and cationic dyes such as Crystal Violet (CV) and Rhodamine B (RB) than the ones that are either anionic (CR) or are smaller in size (MO and MB). The simplicity of the chemical reaction involved to obtain **STNP3** as well as its excellent performance as an adsorbent renders it as a promising porous material for environmental remediation applications. The complementary effects of silsesquioxane and triptycene motifs present in STNPs yield new organic polymeric materials with a high surface area and pore volume. These features in turn are responsible for the highly efficient dye removal capability demonstrated by **STNP3**. These preliminary results indicate that such hybrid materials might play an important role in the development of novel high surface area adsorbents with practical applications in the treatment of wastewater that is contaminated with toxic pollutants.

Experimental section

Materials

All reagents are commercially available and were purchased from either Sigma-Aldrich or Combi-Blocks and used without further purification. 1,2-Dichloroethane was first dried over calcium hydride (CaH_2) and stored with 4 Å molecule sieves before use.

Instrumentation

FTIR spectra of **STNP 1–4** were recorded using a Shimadzu IR Affinity-1 spectrometer. The solid-state ^{13}C cross-polarization magic angle spinning (CP MAS ^{13}C NMR) NMR spectrum of **STNP3** was recorded on a Bruker 400 spectrometer equipped with an 89 mm wide bore and a 9.4 T superconducting magnet with a spinning rate of 12 kHz and CP contact time of 2 ms with a delay time of 2 s. FESEM and EDX were obtained using a Carl Zeiss AG Instrument (Model – SUPRA 55). For PXRD data, a Rigaku TTRAX III X-ray diffractometer was used. Surface area and porosity data were obtained using a Quantachrome Autosorb iQ_2 analyzer. In the gas-sorption experiments, STNPs (80–120 mg) were charged in a bulb cell (stem diameter = 9 mm) and were degassed at 120 °C for 6–8 h by attaching the cell to the degassing unit. Later, the cell (containing the degassed polymer) was filled with He gas and weighed accurately. Sample cells were maintained accurately at different but specific temperatures as per requirement using a KGW isotherm bath (provided by Quantachrome) that was filled with liquid N_2 (77 K), or a temperature-controlled bath (298 K and 273 K). UV-Vis spectra reported in this manuscript were acquired using a Shimadzu UV-2550 UV-Vis spectrophotometer.

Synthesis of STNPs

A typical procedure is described for **STNP3**: OVS (633 mg, 1.0 mmol), anhydrous aluminium chloride (135 mg, 1.0 mmol), triptycene (255 mg, 1.0 mmol), and 1,2-dichloroethane (25 mL) were charged in an oven-dried Schlenk flask. The reaction mixture was stirred at room temperature for 30 min and heated to reflux for 24 h. After cooling to room temperature, the precipitate obtained was filtered and washed with ethanol, THF, water, acetone, and methanol. The products were further purified in a Soxhlet extractor with methanol (for 24 h) and dichloromethane (for 24 h), and then dried in a vacuum oven at 100 °C for 48 h to obtain a yellow powder in good yields (~92%). The obtained solid powder was insoluble in all common solvents.

STNP1, **STNP2**, and **STNP4** were synthesized similarly, with OVS to triptycene molar ratios of 1.0 : 0.53 (OVS 1.0 mmol), 1.0 : 0.86 (OVS 1.0 mmol), and 1.0 : 1.5 (OVS 1.0 mmol), respectively. The final products were collected as a yellow powder with yields of 86% for **STNP1**, 85% for **STNP2** and 89% for **STNP4**.

Conflicts of interest

There are no conflicts to declare.

Acknowledgements

N. D. thanks the Indian Institute of Technology Patna (IIT Patna) for instrumental facilities. A. A., A. H. and R. B. thankfully acknowledge IIT Patna for their respective Institute Research Fellowships.

References

1 G. Singh, J. Lee, A. Karakoti, R. Bahadur, J. Yi, D. Zhao, K. AlBahily and A. Vinu, *Chem. Soc. Rev.*, 2020, **49**, 4360–4404.
2 Y. Zeng, R. Zou and Y. Zhao, *Adv. Mater.*, 2016, **28**, 2855–2873.
3 T. A. Makal, J.-R. Li, W. Lu and H.-C. Zhou, *Chem. Soc. Rev.*, 2012, **41**, 7761–7779.
4 S. Das, P. Heasman, T. Ben and S. Qiu, *Chem. Rev.*, 2017, **117**, 1515–1563.
5 P. Samanta, A. V. Desai, S. Let and S. K. Ghosh, *ACS Sustainable Chem. Eng.*, 2019, **7**, 7456–7478.

6 R.-R. Liang, S.-Y. Jiang, R.-H. A and X. Zhao, *Chem. Soc. Rev.*, 2020, **49**, 3920–3951.
7 Y. Song, Q. Sun, B. Aguila and S. Ma, *Adv. Sci.*, 2019, **6**, 1801410.
8 X. Li, P. Yadav and K. P. Loh, *Chem. Soc. Rev.*, 2020, **49**, 4835–4866.
9 K. Geng, T. He, R. Liu, S. Dalapati, K. T. Tan, Z. Li, S. Tao, Y. Gong, Q. Jiang and D. Jiang, *Chem. Rev.*, 2020, **16**, 8814–8933.
10 J. Wu, F. Xu, S. Li, P. Ma, X. Zhang, Q. Liu, R. Fu and D. Wu, *Adv. Mater.*, 2019, **31**, 1802922.
11 T. Zhang, G. Xing, W. Chen and L. Chen, *Mater. Chem. Front.*, 2020, **4**, 332–353.
12 Y. Byun, S. H. Je, S. N. Talapaneni and A. Coskun, *Chem. – Eur. J.*, 2019, **25**, 10262–10283.
13 D. Xu, J. Guo and F. Yan, *Prog. Polym. Sci.*, 2018, **79**, 121–143.
14 A. Fina, O. Monticelli and G. Camino, *J. Mater. Chem.*, 2010, **20**, 9297–9305.
15 R. M. Laine and M. F. Roll, *Macromolecules*, 2011, **44**, 1073–1109.
16 K. Tanaka and Y. Chujo, *J. Mater. Chem.*, 2012, **22**, 1733–1746.
17 M. Ge and H. Liu, *J. Mater. Chem. A*, 2016, **4**, 16714–16722.
18 D. Wang, W. Yang, S. Feng and H. Liu, *Polym. Chem.*, 2014, **5**, 3634–3642.
19 Q. Wang, H. Liu, C. Jiang and H. Liu, *Polymer*, 2020, **186**, 122004.
20 H. Liu and H. Liu, *J. Mater. Chem. A*, 2017, **5**, 9156–9162.
21 Y. Du, M. Unno and H. Liu, *ACS Appl. Nano Mater.*, 2020, **3**, 1535–1541.
22 X. Yang and H. Liu, *ACS Appl. Mater. Interfaces*, 2019, **11**, 26474–26482.
23 L. Sun, Z. Liang and J. Yu, *Polym. Chem.*, 2015, **6**, 917–924.
24 Y. Zhang, K. Liu, L. Wu, H. Zhong, N. Luo, Y. Zhu, M. Tong, Z. Long and G. Chen, *ACS Sustainable Chem. Eng.*, 2019, **7**, 16907–16916.
25 D. Wang, S. Feng and H. Liu, *Chem. – Eur. J.*, 2016, **22**, 14319–14327.
26 Z. Gou, Y. Zuo, M. Tian and W. Lin, *ACS Appl. Mater. Interfaces*, 2018, **10**, 28979–28991.
27 R. Sun, X. Huo, H. Lu, S. Feng, D. Wang and H. Liu, *Sens. Actuators, B*, 2018, **265**, 476–487.
28 C. Wannasiri, S. Chanmungkalakul, T. Bunchuay, L. Chuenchom, K. Uraisin, V. Ervithayasuporn and S. Kiatkamjornwong, *ACS Appl. Polym. Mater.*, 2020, **2**, 1244–1255.
29 Y. Wu, D. Wang, L. Li, W. Yang, S. Feng and H. Liu, *J. Mater. Chem. A*, 2014, **2**, 2160–2167.
30 C. Zhang, F. Babonneau, C. Bonhomme, R. M. Laine, C. L. Soles, H. A. Hristov and A. F. Yee, *J. Am. Chem. Soc.*, 1998, **120**, 8380–8391.
31 M. Soldatov and H. Liu, *Chem. – Asian J.*, 2019, **14**, 4345–4351.
32 W. Chaikittisilp, A. Sugawara, A. Shimojima and T. Okubo, *Chem. – Eur. J.*, 2010, **16**, 6006–6014.
33 W. Chaikittisilp, A. Sugawara, A. Shimojima and T. Okubo, *Chem. Mater.*, 2010, **22**, 4841–4843.
34 Y. Luo, B. Li, W. Wang, K. Wu and B. Tan, *Adv. Mater.*, 2012, **24**, 5703–5707.
35 C. Zhang, P.-C. Zhu, L. Tan, J.-M. Liu, B. Tan, X.-L. Yang and H.-B. Xu, *Macromolecules*, 2015, **48**, 8509–8514.
36 R. Bera, S. Mondal and N. Das, *Microporous Mesoporous Mater.*, 2018, **257**, 253–261.
37 S. Dey, A. Bhunia, D. Esquivel and C. Janiak, *J. Mater. Chem. A*, 2016, **4**, 6259–6263.
38 H. Tan, Q. Chen, T. Chen and H. Liu, *ACS Appl. Mater. Interfaces*, 2018, **10**, 32717–32725.
39 S. Mondal and N. Das, *J. Mater. Chem. A*, 2015, **3**, 23577–23586.
40 T. B. Schon, A. J. Tilley, E. L. Kynaston and D. S. Seferos, *ACS Appl. Mater. Interfaces*, 2017, **9**, 15631–15637.
41 B. Comesaña-Gándara, J. Chen, C. G. Bezzu, M. Carta, I. Rose, M.-C. Ferrari, E. Esposito, A. Fuoco, J. C. Jansen and N. B. McKeown, *Energy Environ. Sci.*, 2019, **12**, 2733–2740.
42 A. Fuoco, B. Comesaña-Gándara, M. Longo, E. Esposito, M. Monteleone, I. Rose, C. G. Bezzu, M. Carta, N. B. McKeown and J. C. Jansen, *ACS Appl. Mater. Interfaces*, 2018, **10**, 36475–36482.
43 A. Alam, R. Bera, M. Ansari, A. Hassan and N. Das, *Front. Energy Res.*, 2019, **7**, 141.
44 S. Shetty, N. Baig, A. Hassan, S. Al-Mousawi, N. Das and B. Alameddine, *Microporous Mesoporous Mater.*, 2020, **303**, 110256.
45 Y. He, X. Zhu, Y. Li, C. Peng, J. Hu and H. Liu, *Microporous Mesoporous Mater.*, 2015, **214**, 181–187.
46 M. Ansari, A. Alam, R. Bera, A. Hassan, S. Goswami and N. Das, *J. Environ. Chem. Eng.*, 2020, **8**, 103558.
47 Q.-M. Zhang, T.-L. Zhai, Z. Wang, G. Cheng, H. Ma, Q.-P. Zhang, Y.-H. Zhao, B. Tan and C. Zhang, *Adv. Mater. Interfaces*, 2019, **6**, 1900249.
48 T. Xu, Y. He, Y. Qin, C. Zhao, C. Peng, J. Hu and H. Liu, *RSC Adv.*, 2018, **8**, 4963–4968.
49 Y. He, T. Xu, J. Hu, C. Peng, Q. Yang, H. Wang and H. Liu, *RSC Adv.*, 2017, **7**, 30500–30505.
50 N. Baig, S. Shetty, S. Al-Mousawi and B. Alameddine, *Polym. Chem.*, 2020, **11**, 3066–3074.
51 Y. Li, H. Wang, W. Zhao, X. Wang, Y. Shi, H. Fan, H. Sun and L. Tan, *J. Appl. Polym. Sci.*, 2019, **136**, 47987.
52 L. Jia, J. Ma, D. Gao, W. R. T. Tait and L. Sun, *J. Hazard. Mater.*, 2019, **361**, 305–311.
53 D. Borah, S. Rasappa, M. Salaun, M. Zellsman, O. Lorret, G. Liontos, K. Ntetsikas, A. Avgeropoulos and M. A. Morris, *Adv. Funct. Mater.*, 2015, **25**, 3425–3432.
54 F. Alves, P. Scholder and I. Nischang, *ACS Appl. Mater. Interfaces*, 2013, **5**, 2517–2526.
55 T. Ikai, T. Yoshida, K.-I. Shinohara, T. Taniguchi, Y. Wada and T. M. Swager, *J. Am. Chem. Soc.*, 2019, **141**, 4696–4703.
56 R. Bera, M. Ansari, A. Alam and N. Das, *ACS Appl. Polym. Mater.*, 2019, **1**, 959–968.
57 A. Alam, S. Mishra, A. Hassan, R. Bera, S. Dutta, K. Das Saha and N. Das, *ACS Omega*, 2020, **5**, 4250–4260.
58 Q. Liang, S. Cui, S. Xu, C. Yao, M. J. MacLachlan and Z. Li, *Chem. Commun.*, 2018, **54**, 3391–3394.
59 Q.-Q. Dang, X.-M. Wang, Y.-F. Zhan and X.-M. Zhang, *Polym. Chem.*, 2016, **7**, 643–647.

60 W. Chaikittisilp, M. Kubo, T. Moteki, A. Sugawara-Narutaki, A. Shimojima and T. Okubo, *J. Am. Chem. Soc.*, 2011, **133**, 13832–13835.
61 K. Sing, *Pure Appl. Chem.*, 1982, **54**, 2201–2218.
62 X. Yang and H. Liu, *Chem. – Eur. J.*, 2018, **24**, 13504–13511.
63 R. Sun, S. Feng, D. Wang and H. Liu, *Chem. Mater.*, 2018, **30**, 6370–6376.
64 D. Chen, S. Gu, Y. Fu, X. Fu, Y. Zhang, G. Yu and C. Pan, *New J. Chem.*, 2017, **41**, 6834–6839.
65 W. Yang, D. Wang, L. Li and H. Liu, *Eur. J. Inorg. Chem.*, 2014, 2976–2982.
66 Y. Wu, L. Li, W. Yang, S. Feng and H. Liu, *RSC Adv.*, 2015, **5**, 12987–12993.
67 T. M. Swager, *Acc. Chem. Res.*, 2008, **41**, 1181–1189.
68 H. A. Patel, S. Hyun Je, J. Park, D. P. Chen, Y. Jung, C. T. Yavuz and A. Coskun, *Nat. Commun.*, 2013, **4**, 1357.
69 S. Bolisetty, M. Peydayesh and R. Mezzenga, *Chem. Soc. Rev.*, 2019, **48**, 463–487.
70 S. Rojas and P. Horcajada, *Chem. Rev.*, 2020, **120**(16), 8378–8415.
71 I. Ali, *Chem. Rev.*, 2012, **112**, 5073–5091.
72 F. Chen, E. Zhao, T. Kim, J. Wang, G. Hableel, P. J. T. Reardon, S. J. Ananthakrishna, T. Wang, S. Arconada-Alvarez, J. C. Knowles and J. V. Jokerst, *ACS Appl. Mater. Interfaces*, 2017, **9**, 15566–15576.
73 N. Peng, D. Hu, J. Zeng, Y. Li, L. Liang and C. Chang, *ACS Sustainable Chem. Eng.*, 2016, **4**, 7217–7224.
74 N. A. Khan, Z. Hasan and S. H. Jhung, *J. Hazard. Mater.*, 2013, **244–245**, 444–456.
75 X. Zhuang, Y. Wan, C. Feng, Y. Shen and D. Zhao, *Chem. Mater.*, 2009, **21**, 706–716.
76 R. Shen and H. Liu, *RSC Adv.*, 2016, **6**, 37731–37739.
77 W. Shi, S. Tao, Y. Yu, Y. Wang and W. Ma, *J. Mater. Chem.*, 2011, **21**, 15567–15574.
78 Y. Han, W. Li, J. Zhang, H. Meng, Y. Xu and X. Zhang, *RSC Adv.*, 2015, **5**, 104915–104922.